analytical chemistry

ACS AuthorChoice

Article

pubs.acs.org/ac

Open Access on 07/17/2015

Sensitive, Selective Analysis of Selenium Oxoanions Using Microchip Electrophoresis with Contact Conductivity Detection

Scott D. Noblitt,[†] Lucian C. Staicu,[∥,‡] Christopher J. Ackerson,*[,†] and Charles S. Henry*[,†,§,∥]

[†]Chemistry Department, Colorado State University, Fort Collins, Colorado 80523, United States

[‡]Biology Department, Colorado State University, Fort Collins, Colorado 80523, United States

[§]Department of Chemical & Biological Engineering, Colorado State University, Fort Collins, Colorado 80523, United States

[∥]School of Biomedical Engineering, Colorado State University, Fort Collins, Colorado 80523, United States

Supporting Information

ABSTRACT: The common selenium oxoanions selenite (SeO_3^{2-}) and selenate (SeO_4^{2-}) are toxic at intake levels slightly below 1 mg day^{-1}. These anions are currently monitored by a variety of traditional analytical techniques that are time-consuming, expensive, require large sample volumes, and/or lack portability. To address the need for a fast and inexpensive analysis of selenium oxoanions, we present the first microchip capillary zone electrophoresis (MCE) separation targeting these species in the presence of chloride, sulfate, nitrate, nitrite, chlorate, sulfamate, methanesulfonate, and fluoride, which can be simultaneously monitored. The chemistry was designed to give high selectivity in nonideal matrices. Interference from common weak acids is avoided by operating near pH 4. Separation resolution from chloride was enhanced to improve tolerance of high-salinity matrices. As a result, selenate can be quantified in the presence of up to 1.5 mM NaCl, and selenite analysis is even more robust against chloride. Using contact conductivity detection, detection limits for samples with conductivity equal to the background electrolyte are 53 nM (4.2 ppb Se) and 380 nM (30 ppb) for selenate and selenite, respectively. Analysis time, including injection, is ~2 min. The MCE method was validated against ion chromatography (IC) using spiked samples of dilute BBL broth and slightly outperformed the IC in accuracy while requiring <10% of the analysis time. The applicability of the technique to real samples was shown by monitoring the consumption of selenite by bacteria incubated in LB broth.

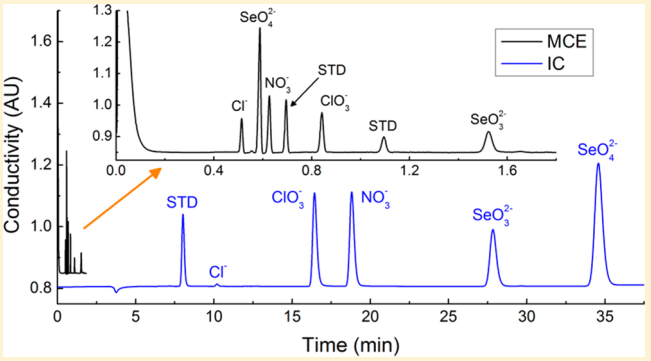

Selenium is an essential trace element with a narrow range between necessary and toxic concentrations.[1,2] A dietary reference intake (DRI) of 55 μg day^{-1} is proposed based on plasma glutathione peroxidase activity as the selenium biomarker.[2] In excess, selenium poisoning (selenosis) can result in neurological pathologies including convulsions, weakness, and decreased cognitive function.[3] Endemic selenosis was reported in China, where maximal intake was estimated at 910 μg day^{-1}.[4] Thus, the window between daily essential and toxic intake is small, at just over 1 order of magnitude. Complicating this picture, selenium speciation versus total selenium intake is crucial.[5] Selenium oxoanions, namely selenite (Se[IV], SeO_3^{2-}) and selenate (Se[VI], SeO_4^{2-}), are water-soluble, bioavailable, and toxic,[6] resulting in a 50 ppb drinking water limit according to the US EPA. The biological and ecological consequences of too little or too much selenium highlight the need for facile analytical methods to determine selenium oxoanion concentration in real-world matrices.

Many analytical techniques can monitor selenium speciation.[7,8] Examples include electrothermal atomic absorption spectrometry (ETAAS), inductively coupled plasma with optical emission spectrometry or mass spectrometry (ICP-OES and ICP-MS), differential pulse cathodic sweeping voltammetry (DPCSV), hydride generation atomic absorption and atomic fluorescence spectrometries (HGAAS and HGAFS), and UV−visible absorbance spectroscopy (after complexation).[8,9] Despite the sensitive, selective, and expensive methods employed for selenium speciation, preconcentration methods such as solid-phase extraction (SPE) are generally required to increase concentrations and/or reduce matrix interference.[9]

Even after extraction and/or preconcentration, a separation step prior to analysis is often necessary for inorganic selenium speciation. Separation techniques include ion chromatography (IC), high-performance liquid chromatography (HPLC), and capillary electrophoresis (CE).[8,10] Chromatographic methods typically exhibit better concentration detection limits, are not as sensitive to high-salinity matrices, and have more-established interfaces to selective detectors. However, chromatography

Received: June 1, 2014
Accepted: July 17, 2014

   dx.doi.org/10.1021/ac502013k | *Anal. Chem.* XXXX, XXX, XXX−XXX

requires larger sample volumes, needs longer analysis times, and can suffer stationary phase damage from matrix species. Stationary-phase sensitivity is especially high for biological matrices. In contrast, CE is suited for selenium speciation due to the ionic nature of the analytes. Compared to chromatography, it requires less sample volume, allows shorter analysis times, and has higher mass sensitivity.[11] Although CE capillaries are prone to fouling by biomacromolecules, capillary replacement is less expensive than replacing chromatographic columns, and there are a variety of CE surface-protection approaches to avoid protein adsorption.[12,13] Additionally, the simple and low-power equipment used in electrophoresis lends this technique to portable applications, particularly when performed as microchip capillary electrophoresis (MCE).[14]

Thus, speed, cost, sample consumption, and portability make CE appealing for inorganic selenium separations. However, CE methods for selenium speciation are limited.[15,16] A few methods employ absorption or indirect fluorescent detection at basic pH.[17−25] This approach is useful for simultaneously monitoring other inorganic oxoanions (e.g., of arsenic and tellurium) and can be optimized to avoid interference from the limited number of common inorganic anions. However, comigrating organic anions can confound selenium oxoanion separations at these conditions, particularly for selenite, due to lack of selectivity in both the separation and detection steps.

Element-specific detection avoids selectivity problems arising with optical and fluorescent detection. Frequently, inductively coupled plasma is used for element-specific detection as either ICP-MS[26−36] or with atomic emission spectrometry (ICP-AES).[26] Direct CE-MS[37,38] and atomic fluorescence spectrometry (CE-AFS)[39] are also utilized. Although these approaches circumvent poor separation selectivity, they require substantially greater operating expense and complexity. An alternative is to use a simple detector coupled with a selective background electrolyte (BGE) that improves separation resolution.

The Kubáň group analyzed selenate, selenite, chloride, sulfate, nitrate, and nitrite in a pH 4 BGE with contactless conductivity detection.[40] At this pH, interference from the majority of organic acids is minimized. Sladkov et al. used an even more acidic BGE (pH 2.5) with CE-UV for selenium speciation in wastewater.[41] At this pH, all common organic acids and most common inorganic weak acids are noninterfering. Although both of these methods achieve selective separation, they use traditional CE. Portability is desirable for environmental monitoring applications. Although portable CE has been repeatedly demonstrated,[42] MCE has a smaller footprint, particularly when coupled to conductivity or electrochemical detection. However, inorganic selenium MCE methods have not yet been developed. The only microchip capillary zone electrophoresis selenium analysis was designed for selenoamino acids.[43] Prest et al. monitored inorganic selenium on a microchip using isotachophoresis and contactless conductivity detection,[44,45] but this had neither suitable resolving power nor detection limits (6−13 μM) for many applications.

Here we report the first MCE system specifically tailored for selective determination of selenate and selenite. Simultaneous monitoring of other strong anions is possible, specifically chloride, sulfate, nitrate, nitrite, chlorate, sulfamate, fluoride, and methanesulfonate. Interference from major organic acids is avoided by using acidic operating conditions (pH 4) under counter electro-osmotic flow (EOF) conditions. Contact conductivity detection is used to achieve low detection limits. The method is designed to maximize robustness against high-chloride matrices, with the selenite analysis being practically unaffected by chloride, and selenate is fully resolved from chloride up to 1.5 mM. For samples with conductivity equal to the separation BGE, selenate and the less-conductive selenite have detection limits of 53 and 380 nM, respectively. Electrophoretic stacking due to sample−BGE conductivity discrepancies further improves detection limits in low-conductivity matrices. Linear ranges span 3−4 orders of magnitude, up to 500 μM for selenite and 1 mM for selenate. The method was tested using samples of dilute (0.5%) BBL broth spiked with known concentrations of selenate, selenite, nitrate, and chlorate. Results agreed with the theoretical values and matched or outperformed IC measurements. The described method will be useful for samples of moderate salinity but relatively low sulfate concentrations.

EXPERIMENTAL SECTION

MCE and IC Materials. MCE BGE chemicals were purchased in the highest purity commercially available. Nicotinic acid and nicotinamide were obtained from Fluka (Buchs, Switzerland). *N*-(2-hydroxyethyl)piperazine-*N*′-(4-butanesulfonic acid) (HEPBS) and *N*-tetradecyl-*N*,*N*-dimethyl-3-ammonio-1-propanesulfonate (TDAPS) came from Sigma-Aldrich (St. Louis, MO). Analytes were obtained at ≥99% purity, unless noted. KCl, $(NH_4)_2SO_4$, $NaNO_3$, $NaNO_2$, and $NaClO_3$ were purchased from Fisher (Fair Lawn, NJ). $Na_2SeO_4{\cdot}10H_2O$, Na_2SeO_3, NaF, $Na_2C_2O_4$, sulfamic acid, sodium methanesulfonate (98%), sodium 1,2-ethanedisulfonate (EDS), sodium pyruvate, malic acid, potassium formate, and tartaric acid were obtained from Sigma-Aldrich. Fumaric acid was procured from Fluka. Trifluoroacetic acid (TFA) was obtained from EMD (Gibbstown, NJ), and malonic acid was purchased from Acros Organics (Geel, Belgium). Ion chromatography was performed using a Metrohm (Riverview, FL) Compact Pro 881 IC, 863 Compact IC Autosampler, MagIC Net 2.2 software, Metrosep A Supp 7 - 250/4.0 column, and suppressed conductivity detection. The isocratic eluent was 3.6 mM Na_2CO_3 (primary standard grade from Sigma-Aldrich) at 0.8 mL min^{-1} and 45 °C. BBL Trypticase Soy Broth was purchased from Becton Dickinson (Sparks, MD). Broth was prepared as directed (30 g/L) and without sterilization. All solutions were prepared using stock chemicals and 18.2 MΩ·cm water from a MilliPore (Billerica, MA) Milli-Q system.

Microchip Construction and Operation. Microchips were prepared in poly(dimethylsiloxane) (PDMS) using a Sylgard 184 kit from Dow Corning (Midland, MI). Device construction was similar to that described in our other work using microwire electrodes and/or contact conductivity detection,[46−48] hence only specific details are given. Figure 1 shows the microchip diagram. Channel lengths (mm) were the following: sample = 10, buffer = 10, waste = 30, separation = 72 (70 effective), and injector = 0.70. Nominal channel widths and heights were 70 and 45 μm, respectively. The detection zone expanded into a 350 μm wide bubble cell to reduce interference from the separation field and increase signal, which is critical for successful contact conductivity detection in MCE.[46] −4330 and −2880 V potentials were applied in the buffer and sample reservoirs, respectively, while keeping the other reservoirs at 0 V. These values generated a nominal −400 V cm^{-1} separation field. During injections, the waste reservoir was set to +1950 V, the sample reservoir −84 V, and the other reservoirs 0 V to fill the double-T injector. Injections were performed for 30 s

dx.doi.org/10.1021/ac502013k | Anal. Chem. XXXX, XXX, XXX−XXX

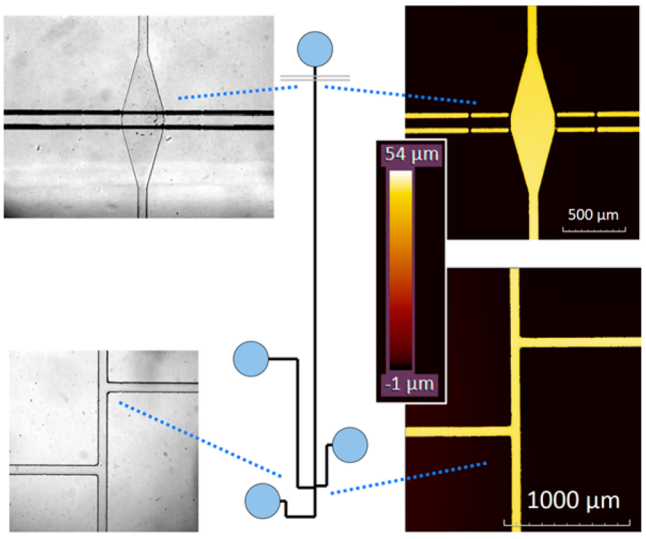

Figure 1. Microchip design used. Reservoir identities clockwise from the top are separation, sample, buffer, and sample waste. Optical profilometry of the mold is shown for the injection and detection zones on the right. Bright-field image are shown on the left. Dimensions are provided in the main text.

(injection time study in Figures S-1 and S-2, Supporting Information). Characterization of the silicon molds with a Zygo (Middlefield, CT) ZeScope optical profilometer showed the channel height to vary between 44 and 56 μm (edge-bead effects induced higher (>50 μm) edge features), and the average width was 74.6 μm. Correcting the calculated separation field using the measured profile gave an estimated −394 V cm^{-1}. Conductivity detection was performed using 30-μm Pt wires (California Fine Wire, Grover Beach, CA). Two parallel Pt wires were placed perpendicular to the channel with 120 μm center-to-center spacing for the conductivity cell.

Data Acquisition and Analysis. All high-voltage potentials were applied using a custom-built, isolated power supply controlled by LabView 8.6 (National Instruments, Austin, TX). Signal was measured using a Dionex (owned by Thermo Scientific, Waltham, MA) CD20 detector, and the 0−1 V analog output was read by a National Instruments USB-6210 DAQ at 2.5 kHz with 125-sample averaging for a 20 Hz effective collection rate. Measured background signal (for BGE 1, described later) was 940 μS cm^{-1} with the CD20 set to a (default) 160 cm^{-1} cell constant. The expected background conductivity was 414 μS cm^{-1}, indicating an actual cell constant of 70 cm^{-1}. This value falls in the expected range from length/area estimates with a lower bound (90 μm edge-to-edge electrode spacing, and channel width/depth of 350 and 49 μm, respectively) of 51 cm^{-1} and upper bound (120 μm center-to-center spacing, 350 μm channel width, and 30 μm electrode "depth") of 114 cm^{-1}. Detector range was 200 μS cm^{-1}; baseline noise was limited by a detector digital-to-analog conversion. The digital resolution was 50.4 μV, equating to 10 nS cm^{-1} on the CD20, 11 ppm of the background. In contrast, the analog noise on each digital step was ∼5 μV. For the limit-of-detection (LOD) study, the LOD signal was considered to be two digital steps.

Raw MCE electropherogram data were analyzed using a custom LabView program. Peak windows were manually entered and drifting baselines (from evaporation and temperature variations) were removed via polynomial subtraction, followed by peak integration. Internal standards are required for reliable quantification in electrophoresis,[49] so calibrations were performed by plotting the analyte/internal standard peak area ratio versus the analyte/standard concentration ratio. For unbiased electrophoresis injections, peak areas are often corrected for EOF drift by dividing by the migration time.[50] However, this method was not employed because the relatively low EOF (∼2 × 10^{-4} cm^2 V^{-1} s^{-1}) was stable. Also, increased migration times from decreased localized electric fields induced by peak overloading (e.g., the high end of the linearity study) led to lower calibration curve correlations with migration-time correction. For IC peak integration, MagIC Net 2.2 was used.

For the MCE linearity study, unweighted linear regressions and correlation coefficients (R^2) were used for evaluation. Because selenium oxoanions are unlikely to be present at high micromolar levels, more rigorous methods for evaluating linear range, such as those recommended by the Analytical Division of the Royal Society,[51] were not employed. For the simulated samples, six aqueous samples were prepared with 0−600 μM nitrate, chlorate, selenate, and selenite (selenium species were varied together because the selenite stock contained measurable selenate). These solutions were mixed in a ∼1:9 ratio with a solution of BGE, internal standard, and BBL broth (spun at 14000 rpm for 10 min with a 30 kDa spin filter) for a final solution of ∼10% sample and 0.5% broth. Both the MCE and IC used six-point, 1−100 μM calibration curves. For MCE, weighted linear regression was employed as recommended for bioanalytical methods.[52] A weighting factor of concentration raised to the −1 power was chosen instead of concentration to the −2 power because the relative concentration uncertainty increased with decreasing concentration. Advantages of weighted regression in analytical measurements have been previously covered.[52−54] For our weighted regressions, methods from these references were used, and the exact procedure is covered in the Supporting Information. For IC calibration, a second-order polynomial weighted regression was used because suppressed IC is fundamentally nonlinear.[55,56] The MCE analysis of the bacterial consumption of selenite and nitrate in LB broth was performed similarly to the BBL broth analysis. The only significant difference was a 250× dilution used instead of the 200× dilution.

Data-analysis procedures for analyzing the HEPBS and TDAPS studies are described in the Supporting Information. Briefly, PeakMaster 5.2 simulations were used to calculate the mobility of sulfamate, which does not strongly interact with either additive. The predicted mobility was modified to account for viscosity differences (electrophoretic mobility is inversely proportional to viscosity) and used to calculate the EOF. This EOF was used to compute analyte electrophoretic mobilities, and these mobilities were adjusted to be representative of water at 25 °C for plotting and fitting of affinity constants.

RESULTS AND DISCUSSION

Background Electrolyte Development. We chose conductivity detection to monitor analyte elution because it is inexpensive, relatively portable, and has been demonstrated to routinely provide submicromolar detection limits. Given that conductivity detection, like indirect UV-absorbance, is indiscriminant, selectivity arises entirely from the electrophoretic separation. Selenate is easily resolvable from organic acids with MCE due to its high mobility. Only similarly mobile inorganic species, specifically chloride, sulfate, nitrate, and nitrite, may interfere with selenate. However, selenite, even when fully

dx.doi.org/10.1021/ac502013k | Anal. Chem. XXXX, XXX, XXX−XXX

deprotonated, comigrates with potentially dozens of organic acids common in biological matrices, depending on the pH.[57] However, selenite's lower pK_a (2.6) is significantly below most organics (>4), permitting the slower biselenite anion to be analyzed at conditions between its lower pK_a and the pK_a of most organic acids, yielding fewer potential interferents. Despite the benefits of this low-pH approach, only two reports have demonstrated its utility, one at pH 2.5,[41] and the other at pH 4.0.[40] Previously, our group demonstrated that pyridine carboxylic acid electrolytes are highly compatible with contact conductivity detection and this low-pH approach.[46] We further improved selectivity by adding zwitterionic surfactants to the BGE,[47] eliminating interference from weakly solvated anions, and this approach has been imitated in other work.[58−60] Finally, our group demonstrated that protonated diamines, even as zwitterions, exhibit selective interaction with dianions,[61] and this can be exploited as another separation development tool.[47,62] Consequently, the combination of a pyridine carboxylic acid, diamine-containing base, and zwitterionic surfactant at a pH near 4 were chosen for shaping the desired separation.

Ions relevant for the current separation include chloride, sulfate, nitrate, nitrite, chlorate, fluoride, and formate. Of these, only nitrite, fluoride, and formate are significantly affected by pH in the pH-4 regime. Organic ions with high electrophoretic mobility at this pH were also considered, specifically oxalate, malonate, tartrate, fumarate, and pyruvate. Although phosphate is often present, its expected migration time is much later than that of selenite at the BGE pH according to PeakMaster simulations.[57] The mobility of all the weak acids can be modified easily via pH. Similarly, ionic strength allows altering relative mobilities of mono- and dianions, although its range is limited (∼1−10 mM) by buffering and stacking considerations on the low end and background conductivity on the high end of concentration ranges. Methodical studies on pH and ionic strength were not performed because their effects are predictable with PeakMaster simulations.[57] Instead, these variables were used as tweaks to the separation after optimizing the zwitterionic surfactant and diamine complexation.

The purpose of the zwitterionic surfactant is to alter the mobility of weakly solvated anions through interaction with surfactant micelles. The surfactant also stabilizes the EOF. On the basis of previous work,[47] TDAPS was chosen due to its purity, selectivity, and low critical micelle concentration. A TDAPS concentration study was performed at a calculated ionic strength of 5.0 mM and pH 4.00 (measured = 3.95). Figure 2a shows the resulting electrophoretic mobilities. In addition to the previously mentioned ions, the following potential internal standards were evaluated: EDS, 1,3-propane-disulfonate (PDS), sulfamate, methanesulfonate, and TFA. Interaction strength with the TDAPS micelles qualitatively agreed with the reported trends of weakly solvated anions partitioning more favorably, showing selectivity that follows the Hofmeister series.[63] Nitrate, chlorate, and TFA exhibited the strongest interactions with TDAPS, and respective association constants were measured at 5.2, 12.8, and 14.4 M^{-1} (all measured affinity constants are provided in Table S-1, Supporting Information).

The BGE diamine is added to achieve control over the mobility of the dianionic analytes (sulfate and selenate). It also acts as a buffering base/cation. Although most protonated diamines are capable of altering dianion mobility,[61] to keep conductivity low, reduce ion-depletion effects, and increase

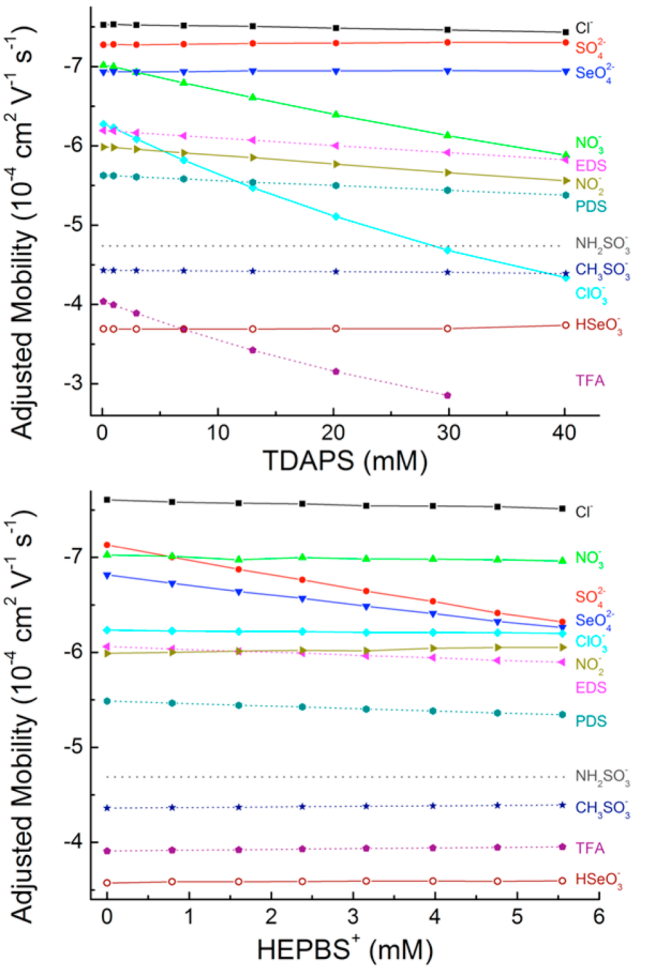

Figure 2. Electrophoretic mobilities as a function of concentration for (top) TDAPS and (bottom) HEPBS. Solid lines are for analyte species, and dotted lines are for potential internal standards.

buffer capacity, zwitterionic diamines with pK_a values near the operating pH are preferable. Previously, we found HEPBS to work well for these purposes,[47] so it was chosen. However, in previous separations, the diamine was used as the sole base because the desired complexation, pH, and ionic strength were conveniently achieved with a single base.[47,62] Because of the proximity of selenate and sulfate in this work, another base was needed because ionic strength and protonated diamine concentration needed to be varied independently. Ionic strength affects all dianions uniformly, whereas diamine concentration imparts some selectivity. Therefore, nicotinamide was chosen as the second BGE base due to its high commercial purity, solubility, pK_a, and moderately low molar conductivity. A quantitative study on electrophoretic mobility as a function of HEPBS concentration was performed using nicotinamide as a cobase at a calculated ionic strength of 7.5 mM and pH 4.00 (measured = 3.98). Results are shown in Figure 2b. The expected trends of complexation with sulfate/selenate and no significant interaction with the monoanions were observed. The precision of the data is lower than in the TDAPS study, possibly due to increased and variable joule heating at the higher ionic strength and differing conductivities of the BGEs. This leads to artifacts such as slight increases in the observed mobilities of some monoanions. The data quality precluded evaluating affinity constants for the weaker interactions, but

dx.doi.org/10.1021/ac502013k | Anal. Chem. XXXX, XXX, XXX−XXX

sulfate and selenate were measured at 34.4 and 23.8 M^{-1}, respectively. The relative strengths of these two interactions qualitatively agree with previous studies,[61] and their magnitudes are 2−2.5× higher, which is expected for the lower ionic strength used here (7.5 vs 30 mM). Somewhat surprisingly, little complexation was observed for the dianionic EDS and PDS. This low affinity was not explored but may be due to the separation of the charged moieties in these species. The HEPBS results indicate that sulfate/selenate resolution decreases with added HEPBS, so the only benefit of including HEPBS is to increase resolution with chloride. Optimized conditions require balancing sulfate/selenate resolution with avoiding an overloaded chloride peak present in some samples.

Combining the results from Figure 2 with well-known pH and ionic strength effects allowed us to develop three optimized conditions, and example separations with 10 μM analytes are shown in Figure 3. The top trace was performed with BGE 1,

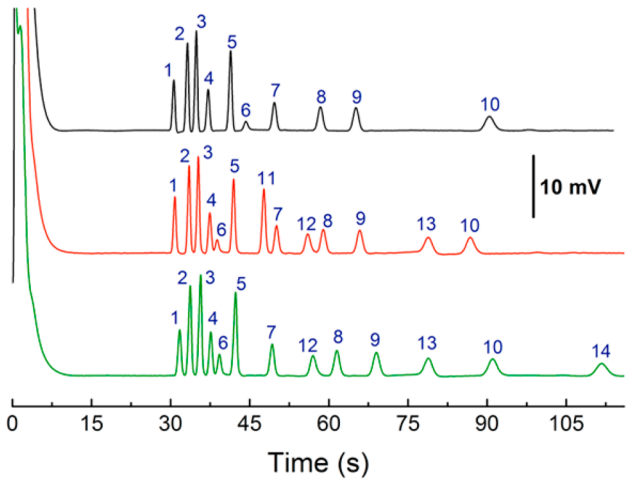

Figure 3. Possible separations obtainable with the BGE systems (concentrations provided in the main text). Top to bottom: BGE 1, BGE 2, and BGE 3. Identities: 1, chloride; 2, sulfate; 3, selenate; 4, nitrate; 5, EDS (standard); 6, nitrite; 7, chlorate; 8, sulfamate; 9, methanesulfonate; 10, selenite; 11, PDS (standard); 12, fluoride; 13, formate; 14, TFA (standard).

which consists of 42 mM nicotinic acid, 15 mM nicotinamide, 2.6 mM HEPBS, and 18 mM TDAPS. Calculated ionic strength, pH, and conductivity are 6.4 mM, 3.95, and 414 μS cm^{-1}, respectively. These conditions are favored for being highly selective. Drawbacks of this BGE include fluoride/methanesulfonate comigration and long formate migration times (electropherograms in Figure S3, Supporting Information). Also, the nitrite peak is less intense than expected for conductivity detection. Inspection of the nitrite peak reveals tailing. Because nitrite peak shape and intensity improve at higher pH, we concluded that the protonated fraction undergoes significant interaction with the PDMS substrate. To improve nitrite sensitivity, resolve fluoride, and speed up formate, a higher pH can be used, although this decreases selectivity against organic interferents. BGE 2, the second trace of Figure 3, utilizes a higher pH. Its composition is 25 mM nicotinic acid, 36 mM nicotinamide, 3.8 mM HEPBS, and 18 mM TDAPS, yielding a calculated 6.4 mM ionic strength, 395 μS cm^{-1} conductivity, and pH 4.22. A modest increase in nitrite sensitivity and resolution of both fluoride and formate are obtained. The higher mobility of nitrite also improves PDS as an internal standard because nitrite's reduced tailing causes less interference. As already mentioned, the main drawback of increasing pH is the greater susceptibility to interfering organic compounds. The final trace in Figure 3 shows BGE 3, which is composed of 12 mM nicotinic acid, 14 mM nicotinamide, 4 mM HEPBS, and 12 mM TDAPS. The calculated ionic strength, pH, and conductivity are 3.1 mM, 4.30, and 200 μS cm^{-1}, respectively. The main differences in BGE 2 and BGE 3 are ionic strength and conductivity. BGE 3 has approximately half the ionic strength and conductivity. This leads to a decrease in resolution between chloride and both sulfate and selenate, making it less suitable for high-chloride matrices. However, the advantage of BGE 3 is its improved conductivity detection. With the detector used here, the lower background conductivity reduced the digital step size, doubling signal-to-noise ratio. Overall, the choice of BGE is application-dependent, but BGE 1 is recommended for most applications.

Method Figures of Merit. Method detection limits are of primary importance in selenium assays because of the low concentrations. In electrophoresis with electrokinetic injection, the injected quantity depends on the sample conductivity because of field-amplified stacking effects, with the injected amount being roughly proportional to the BGE/sample conductivity ratio. For this work, the detection limits (and linear ranges) were measured using BGE 1 for samples prepared in BGE to eliminate stacking effects. Limits of detection were 53 nM (4.2 ppb Se) for selenate and 380 (30 ppb Se) for selenite. For the other analytes in the top trace of Figure 3, limits of detection were 140−240 nM except for chloride (1.9 μM) and nitrite (610 nM). A table of the determined detection limits for all species is provided in Table S-2 (Supporting Information). Detection limits are dictated by the instrument digital−analog conversion except for chloride, sulfate, nitrate, and methanesulfonate, which had significant blanks that were measurable above the baseline, and were therefore measured as 3σ of blanks. Overall, the selenium detection limits are better than those reported for CE with nonspecific detectors, such as indirect UV, indirect fluorescent, and contactless conductivity detection,[18,19,40] but cannot compete with the more expensive ICP and MS detectors.

To test linear ranges, 10 μM EDS was used as an internal standard and the peak area ratio was measured for eight concentrations from ∼1−1000 μM. Linearity below 1 μM was not specifically evaluated, but response was observed to be linear to the LOD in the detection limit study, where multiple concentrations were analyzed below 1 μM. Linearity for chloride, nitrate, and sulfamate was only tested to 500 μM because these three species were analyzed together and nitrate/EDS resolution was incomplete at 1000 μM. All species maintained linearity for the entire tested range except selenite, which showed reduced sensitivity at 1000 μM. It is unknown why there was a reduction in sensitivity for only selenite above 500 μM, but it may stem from the injection, as selenite reaches the injector later than the other species. Regardless, linearity to only 500 μM is unlikely problematic for selenite since few samples present selenite this high and those that do can be diluted. Correlation coefficients for the linear fits were >0.9999 except for chloride (0.9998), selenite (0.9990), and nitrite (0.9985). The lower precision for these three species was attributed, respectively, to ubiquity (more variable blanks), a broader peak (variable integration width), and peak tailing.

Performance in Realistic Matrices. The most prevalent ions in most matrices, particularly biological ones, are sodium

dx.doi.org/10.1021/ac502013k | Anal. Chem. XXXX, XXX, XXX−XXX

and chloride. They interfere with analysis by increasing matrix conductivity, and high chloride manifests as an overloaded peak that can overwhelm smaller peaks. To test robustness against chloride interference, the separation of 10 μM species in BGE 1 was performed with 11 NaCl concentrations ranging from 0 to 3 mM (Figure 4). Sulfate remains resolved to 0.5 mM chloride,

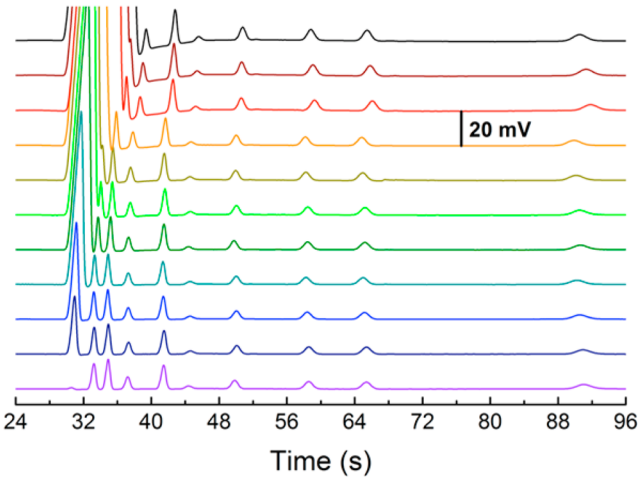

Figure 4. Effect of chloride on BGE 1 separation. Peaks are the first ten identified in Figure 3. Chloride concentrations (mM, from bottom): 0.00, 0.05, 0.10, 0.25, 0.50, 0.75, 1.0, 1.5, 2.0, 2.5, and 3.0. Other species were 10 μM.

selenate is resolved through 1.5 mM, and nitrate stays resolved to 3.0 mM. The slower peaks are practically unaffected by these levels of chloride, as expected. The most significant problem from high chloride is the large baseline perturbation, particularly for concentrations >1 mM. We suspect this problem is due to small levels of contaminant chloride (and possibly sulfate) present in the BGE constituents rather than a fundamental issue with the BGE or detector, as a small baseline perturbation is present even in the absence of sample chloride. Despite the perturbation, the durability of the separation against chloride is sufficient for many matrix types, although most biological samples will need dilution prior to analysis.

Because of the relatively slow migration of biselenite, it is prone to interference from weak acids. Therefore, BGE 1 was tested for interference from fluoride, formate, oxalate, malonate, tartrate, fumarate, and pyruvate (see Figure S-3, Supporting Information). As already mentioned, fluoride comigrates with methanesulfonate, and formate is significantly slower than selenite (by ~30 s). Oxalate did not give a peak, and malonate exhibited a broad, tailing peak beginning ~10 s after selenite. The poor behavior of these ions is attributed to their ligand qualities leading to them adsorbing to bound metals on the capillary surface. This behavior has been observed for polyvalent anions on fused silica,[64] and we previously observed reduced oxalate sensitivity with PDMS devices and remedied it using a metal-binding BGE.[47] Fumarate and tartrate comigrate with formate. Pyruvate appears as a tailing peak ~10 s before selenite, but does not interfere significantly. These anions are the most common interferents, but other organics could pose an issue for specific applications and would need to be tested.

In addition to ionic species, nonionic species could potentially interfere with quantification. To test the resilience of BGE 1 to a realistic matrix, six artificial samples containing known amounts of selenate, selenite, nitrate, and chlorate were prepared in 0.5% BBL broth and analyzed with both MCE and IC. The final matrix contained ~430 μM chloride, ~72 μM phosphate, and a range of biomolecules including sugars and protein fragments. Results are shown in Table 1, and

Table 1. Expected and Measured Concentrations (μM) for Dilute BBL Broth[a]

ID	selenate	selenite	nitrate	chlorate
Smp1	0	0	0	0
IC	BDL[b]	BDL	BDL	BDL
MCE	BDL	BDL	BDL	BDL
Smp 2	166.6	166.9	9.6	68.2
IC	163 (13)[c]	**190 (12)**[d]	11.0 (5.2)	66.5 (7.2)
MCE	168.9 (4.1)	172 (16)	11.4 (2.1)	70.3 (8.2)
Smp 3	9.7	9.7	69.2	301.8
IC	11.9 (5.6)	**4.0 (4.7)**	67.7 (7.2)	306 (18)
MCE	10.8 (1.3)	8.6 (4.8)	67.6 (4.0)	299 (17)
Smp 4	69.6	69.7	306.5	589.4
IC	67.0 (7.3)	**88.1 (7.2)**	301 (19)	591 (22)
MCE	71.2 (2.7)	68 (10)	304.6 (8.5)	584 (25)
Smp 5	306.5	307.1	594.9	9.6
IC	303 (19)	**330 (16)**	599 (22)	10.2 (5.4)
MCE	305.9 (5.7)	314 (22)	594 (13)	10.1 (4.1)
Smp 6	596.4	597.5	168.6	167.5
IC	598 (22)	**626 (19)**	167 (13)	163 (13)
MCE	601.2 (8.4)	608 (32)	**177.0 (6.5)**	168 (12)

[a]Solutions diluted 10× into final solution containing 0.5% BBL broth. [b]BDL: below detection limit. [c]Parenthetical values: 95% confidence interval half widths. [d]Bold values: expected concentration outside the confidence interval.

representative separations are given in Figures S-4 and S-5 (Supporting Information). Our MCE method correctly quantified 23 of 24 measurements, with one nitrate value differing at the 95% confidence interval (but falling within the 99% interval). The IC method agreed with the expected values for all selenate, nitrate, and chlorate measurements, but all the nonzero selenite samples were outside the 95% confidence interval. The reason was selenite's placement in the IC separation, shortly after a tailing phosphate peak. Phosphate's tail altered the integration of selenite, making it significantly different from the calibration. However, the IC's failure to properly analyze selenite here is due to the employed method and not an inherent shortcoming of IC. To properly compare MCE and IC, the average error for the other species was considered, excluding values below the LOD. For this data subset (n = 15), MCE averaged 2.3 μM and 3.2% error; IC averaged 2.6 μM and 4.2% error. The slightly superior MCE results are also evident from their smaller confidence intervals, in part a consequence of the additional calibration degree of freedom.

The BGE 1 method was further evaluated by monitoring anion consumption by a strain of *pseudomonas* bacteria cultured in LB broth spiked with nitrate (21.3 mM) and selenite (12.7 mM). After the 250× dilution, nitrate was 85 μM, selenite was initially at 51 μM, and the matrix contained ~680 μM chloride. Electropherograms and analyte concentrations as a function of

dx.doi.org/10.1021/ac502013k | *Anal. Chem.* XXXX, XXX, XXX–XXX

incubation time are shown in Figure 5. The separation maintained integrity despite the complex matrix, and no

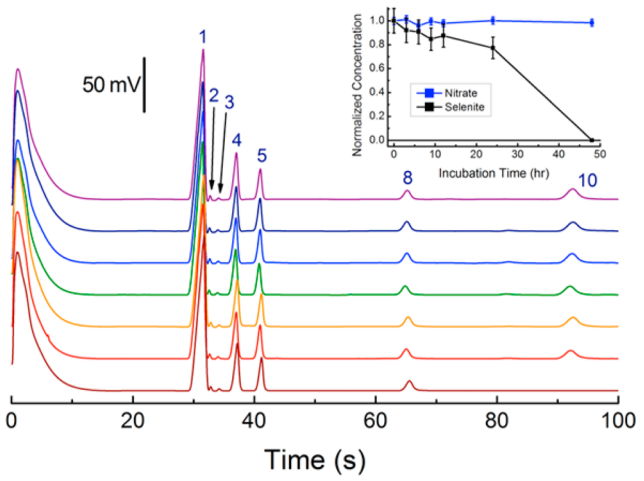

Figure 5. Bacteria consumption of selenite monitored by MCE with BGE 1. Peaks identities are as given in Figure 3. Incubation time (in hours, from top): 0, 3, 6, 9, 12, 24, and 48. Internal standards were 40 μM. Inset concentrations were normalized to the starting concentrations.

significant peaks were observed after selenite (LB broth does not contain phosphate). The bacteria's preference for selenite over nitrate is apparent, with the concentration of nitrate not changing significantly while the concentration of selenite decreased until it was below the detection limit after 48 h of incubation. Overall, this application shows the utility of this technique for measuring selenium oxoanions in realistic biological matrices.

Limitations and Avenues for Improvement. Although the demonstrated method is durable and highly quantitative, it has several shortcomings. The primary restraint is the moderate resolution between selenate and sulfate (~1.8 for 10 μM ions). For biological matrices, this may not be an issue, but many high-selenium matrices also have high levels of sulfate. Although HEPBS improves resolution from chloride, it lowers sulfate/selenate resolution due to its higher sulfate affinity (14.8 vs 9.3 M^{-1}),[61] limiting the amount of complexation that can be employed. Ideally, a diamine with preference for selenate is preferable; unfortunately, there are currently no known diamines with this selectivity.[61] The best available option would be to use bis-tris propane because of its similar affinities for sulfate and selenate (17.2 and 15.0 M^{-1}, respectively),[61] so little resolution would be lost. However, background conductivity and ion depletion rate would increase with bis-tris propane, whereas buffering capacity would decrease.

Another limitation of the separation is the baseline perturbation near the chloride peak. This is attributed to low-level impurities (chloride and/or sulfate) present in the employed buffers. The impurities act as BGE co-ions, and multiple co-ions induce system zone(s) in the separation. The relatively low impurity concentration results in the system zone being located near the mobility of the impurity ion.[65] These impurities also lead to high blank values for chloride and sulfate, raising their detection limits. Purifying these buffers or replacing them with higher purity ones would improve performance. With better buffer purity, higher ionic strengths could also be employed for resolution from chloride instead of using a diamine, increasing sulfate/selenate resolution. That approach would be limited by increasing BGE conductivity, which lowers conductivity detection performance and increases resistive heating effects.

The final major drawback of this method is its concentration sensitivity. Although the low-ppb detection limits compare well with other electrophoretic selenium separations with non-selective detectors, they are insufficient for measuring trace species in high-chloride matrices. This limits the application space of the separation to those with only low-millimolar chloride content, with selenium concentrations high enough to undergo significant dilution, or to applications amendable to extraction/preconcentration procedures (which are frequently used for selenium monitoring).[9] One way to curb this limitation is to develop an optimized conductivity detector for MCE. The current detector is limited by a digital−analog conversion. One future research goal in our lab is to design a specialized contact conductivity detector for MCE. With an optimized detector, mass detection limits would decrease, permitting smaller injections and therefore less overloaded chloride peaks.

CONCLUSIONS

We demonstrated an MCE approach for the selective and sensitive monitoring of selenium oxoanions and other inorganic anions using contact conductivity detection. The ppb-level detection limits are adequate for many applications, the method can tolerate chloride concentrations up to ~1.5 mM before losing selenate resolution, and interference from common organic acids is avoided. The durability of the separation was confirmed using samples in dilute biological media, where analysis quality was maintained. However, the combination of sensitivity and resilience to salinity is not high enough to perform trace analysis in biological matrices without an extraction/preconcentration step. The major method limitations and some options for improvement were discussed. Overall, the method provides an inexpensive and fast option to traditional selenium monitoring approaches for many applications.

ASSOCIATED CONTENT

Supporting Information

Additional details on the following: injection time, affinity constant analysis and results, organic interferents, measured detection limits, and simulated sample analysis and statistical workup. This material is available free of charge via the Internet at http://pubs.acs.org.

AUTHOR INFORMATION

Corresponding Authors

*C. S. Henry. Address: Chemistry Department, 1872 Campus Delivery, Fort Collins, CO 80523, USA. E-mail: chuck.henry@colostate.edu.

*C. J. Ackerson. E-mail: ackerson@mail.colostate.edu.

Present Address

[‖]University Paris Est, 5 Boulevard Descartes, 77454 Marne-la-Vallee, France.

Author Contributions

The paper was written through contributions of all authors. All authors have given approval to the final version of the paper.

dx.doi.org/10.1021/ac502013k | *Anal. Chem.* XXXX, XXX, XXX−XXX

Funding

C.J.A. acknowledges funding support from NIH R21 EB014520. This research was conducted while C.J.A. was a New Investigator in Alzheimer's Disease Grant recipient from the American Federation for Aging Research.

Notes

The authors declare no competing financial interest.

■ ACKNOWLEDGMENTS

We thank Professor Elizabeth Pilon-Smits of Colorado State University and the Fulbright Commission for supervising and financing Lucian Staicu's research.

■ REFERENCES

(1) Barceloux, D. G. *J. Toxicol., Clin. Toxicol.* **1999**, *37*, 145−172.
(2) Levander, O. A.; Burk, R. F. Update of human dietary standards for selenium. In *Selenium - Its Molecular Biology and Role in Human Health*; Hatfield, D. L., Berry, M. J., Gladyshev, V. N., Eds.; Springer: New York, 2006; pp 399−410.
(3) Tinggi, U. *Toxicol. Lett.* **2003**, *137*, 103−110.
(4) Yang, G.; Yin, S.; Zhou, R.; Gu, L.; Yan, B.; Liu, Y.; Liu, Y. *J. Trace Elem. Electrolytes Health Dis.* **1989**, *3*, 123−130.
(5) Rayman, M. P.; Infante, H. G.; Sargent, M. *Br. J. Nutr.* **2008**, *100*, 238−253.
(6) Simmons, D. B. D.; Wallschlager, D. *Environ. Toxicol. Chem.* **2005**, *24*, 1331−1343.
(7) Połatajko, A.; Jakubowski, N.; Szpunar, J. *J. Anal. At. Spectrom.* **2006**, *21*, 639−654.
(8) Uden, P. C. *Anal. Bioanal. Chem.* **2002**, *373*, 422−431.
(9) Latorre, C. H.; García, J. B.; Martín, S. G.; Crecente, R. M. P. *Anal. Chim. Acta* **2013**, *804*, 37−49.
(10) Uden, P. C.; Boakye, H. T.; Kahakachchi, C.; Tyson, J. F. *J. Chromatogr. A* **2004**, *1050*, 85−93.
(11) Pacáková, V.; Štulík, K. *J. Chromatogr. A* **1997**, *789*, 169−180.
(12) Liu, J. K.; Lee, M. L. *Electrophoresis* **2006**, *27*, 3533−3546.
(13) Lucy, C. A.; MacDonald, A. M.; Gulcev, M. D. *J. Chromatogr. A* **2008**, *1184*, 81−105.
(14) Manz, A.; Harrison, D. J.; Verpoorte, E. M. J.; Fettinger, J. C.; Paulus, A.; Ludi, H.; Widmer, H. M. *J. Chromatogr.* **1992**, *593*, 253−258.
(15) Pyrzyńska, K. *Talanta* **2001**, *55*, 657−667.
(16) Morales, R.; Lopez-Sańchez, J. F.; Rubio, R. *TrAC, Trends Anal. Chem.* **2008**, *27*, 183−189.
(17) Casiot, C.; Alonso, M. C. B.; Boisson, J.; Donard, O. F. X.; Potin-Gautier, M. *Analyst* **1998**, *123*, 2887−2893.
(18) Chang, S. Y.; Chiang, H. T. *Electrophoresis* **2002**, *23*, 2913−2917.
(19) Dzierzgowska, M.; Pyrzyńska, K.; Pobozy, E. *J. Chromatogr. A* **2003**, *984*, 291−295.
(20) Li, K.; Li, S. F. Y. *Analyst* **1995**, *120*, 361−366.
(21) Gilon, N.; PotinGautier, M. *J. Chromatogr. A* **1996**, *732*, 369−376.
(22) Walker, E. B.; Walker, J. C.; Zaugg, S. E.; Davidson, R. *J. Chromatogr. A* **1996**, *745*, 111−115.
(23) Hagege, A.; Troyer, C.; Grasserbauer, M.; Leroy, M. J. F. *Mikrochim. Acta* **1997**, *127*, 113−118.
(24) Duan, J. K.; Hu, B.; He, M. *Electrophoresis* **2012**, *33*, 2953−2960.
(25) Pathem, B. K.; Pradenas, G. A.; Castro, M. E.; Vásquez, C. C.; Chasteen, T. G. *Anal. Biochem.* **2007**, *364*, 138−144.
(26) Deng, B. Y.; Feng, J. R.; Meng, J. *Anal. Chim. Acta* **2007**, *583*, 92−97.
(27) Bendahl, L.; Gammelgaard, B.; Jøns, O.; Farver, O.; Hansen, S. H. *J. Anal. At. Spectrom.* **2001**, *16*, 38−42.
(28) Casiot, C.; Donard, O. F. X.; Potin-Gautier, M. *Spectrochim. Acta, Part B* **2002**, *57*, 173−187.
(29) Kannamkumarath, S. S.; Wrobel, K.; Wuilloud, R. G. *Talanta* **2005**, *66*, 153−159.
(30) Magnuson, M. L.; Creed, J. T.; Brockhoff, C. A. *Analyst* **1997**, *122*, 1057−1061.
(31) Michalke, B. *Spectroscopy* **2000**, *15*, 30−+.
(32) Michalke, B.; Schramel, O.; Kettrup, A. *Fresenius' J. Anal. Chem.* **1999**, *363*, 456−459.
(33) Michalke, B.; Schramel, P. *Electrophoresis* **1998**, *19*, 270−275.
(34) Michalke, B.; Schramel, P. *J. Chromatogr. A* **1998**, *807*, 71−80.
(35) Mounicou, S.; McSheehy, S.; Szpunar, J.; Potin-Gautier, M.; Lobinski, R. *J. Anal. At. Spectrom.* **2002**, *17*, 15−20.
(36) Zhao, Y. Q.; Zheng, J. P.; Yang, M. W.; Yang, G. D.; Wu, Y. N.; Fu, F. F. *Talanta* **2011**, *84*, 983−988.
(37) Corr, J. J.; Anacleto, J. F. *Anal. Chem.* **1996**, *68*, 2155−2163.
(38) Zhang, H. J.; Gavina, J.; Feng, Y. L. *J. Chromatogr. A* **2011**, *1218*, 3095−3104.
(39) Lu, C. Y.; Yan, X. P. *Electrophoresis* **2005**, *26*, 155−160.
(40) Kubáň, P.; Kubáň, P.; Kubáň, V. *Anal. Bioanal. Chem.* **2004**, *378*, 378−382.
(41) Sladkov, V.; Fourest, B.; David, F.; Venault, L.; Lecomte, M. *Anal. Bioanal. Chem.* **2003**, *376*, 455−459.
(42) Ryvolová, M.; Preisler, J.; Foret, F.; Hauser, P. C.; Krasensky, P.; Paull, B.; Macka, M. *Anal. Chem.* **2010**, *82*, 129−135.
(43) Wang, J.; Mannino, S.; Camera, C.; Chatrathi, M. P.; Scampicchio, M.; Zima, J. *J. Chromatogr. A* **2005**, *1091*, 177−182.
(44) Prest, J. E.; Baldock, S. J.; Fielden, P. R.; Goddard, N. J.; Brown, B. J. T. *Anal. Bioanal. Chem.* **2003**, *376*, 78−84.
(45) Prest, J. E.; Baldock, S. J.; Fielden, P. R.; Goddard, N. J.; Brown, B. J. T. *Microchim. Acta* **2005**, *151*, 223−230.
(46) Noblitt, S. D.; Henry, C. S. *Anal. Chem.* **2008**, *80*, 7624−7630.
(47) Noblitt, S. D.; Schwandner, F. M.; Hering, S. V.; Collett, J. L.; Henry, C. S. *J. Chromatogr. A* **2009**, *1216*, 1503−1510.
(48) Liu, Y.; Vickers, J. A.; Henry, C. S. *Anal. Chem.* **2004**, *76*, 1513−1517.
(49) Altria, K. D.; Fabre, H. *Chromatographia* **1995**, *40*, 313−320.
(50) Hjertén, S.; Elenbring, K.; Kilár, F.; Liao, J. L.; Chen, A. J. C.; Siebert, C. J.; Zhu, M. D. *J. Chromatogr.* **1987**, *403*, 47−61.
(51) Thompson, M.; Brown, D. W.; Fearn, T.; Gardner, M. J.; Greenhow, E. J.; Howarth, R.; Miller, J. N.; Newman, E. J.; Ripley, B. D.; Swan, K. J.; Williams, A.; Wood, R.; Wilson, J. J. *Analyst* **1994**, *119*, 2363−2366.
(52) Almeida, A. M.; Castel-Branco, M. M.; Falcão, A. C. *J. Chromatogr. B* **2002**, *774*, 215−222.
(53) Garden, J. S.; Mitchell, D. G.; Mills, W. N. *Anal. Chem.* **1980**, *52*, 2310−2315.
(54) Miller, J. N. *Analyst* **1991**, *116*, 3−14.
(55) Midgley, D.; Parker, R. L. *Talanta* **1989**, *36*, 1277−1283.
(56) Brinkmann, T.; Specht, C. H.; Frimmel, F. H. *J. Chromatogr. A* **2002**, *957*, 99−109.
(57) Jaroš, M.; Včeláková, K.; Zusková, I.; Gaš, B. *Electrophoresis* **2002**, *23*, 2667−2677.
(58) Noblitt, S. D.; Lewis, G. S.; Liu, Y.; Hering, S. V.; Collett, J. L.; Henry, C. S. *Anal. Chem.* **2009**, *81*, 10029−10037.
(59) Gertsch, J. C.; Noblitt, S. D.; Cropek, D. M.; Henry, C. S. *Anal. Chem.* **2010**, *82*, 3426−3429.
(60) Kubáň, P.; Kiplagat, I. K.; Boček, P. *Electrophoresis* **2012**, *33*, 2695−2702.
(61) Noblitt, S. D.; Speights, R. M.; Henry, C. S. *Electrophoresis* **2011**, *32*, 2986−2993.
(62) Noblitt, S. D.; Mazzoleni, L. R.; Hering, S. V.; Collett, J. L.; Henry, C. S. *J. Chromatogr. A* **2007**, *1154*, 400−406.
(63) Cook, H. A.; Hu, W. Z.; Fritz, J. S.; Haddad, P. R. *Anal. Chem.* **2001**, *73*, 3022−3027.
(64) Gassner, B.; Friedl, W.; Kenndler, E. *J. Chromatogr. A* **1994**, *680*, 25−31.
(65) Beckers, J. L.; Bocek, P. *Electrophoresis* **2003**, *24*, 518−535.

Supporting Information for:
Sensitive, Selective Analysis of Selenium Oxoanions Using Microchip Electrophoresis with Contact Conductivity Detection

Analytical Chemistry Manuscript

Authors
Scott D. Noblitt, Lucian Staicu, Christopher J. Ackerson, Charles S. Henry
Colorado State University, Fort Collins, CO, 80523, USA

Abstract
This supporting information file expounds upon several areas of the main text. A description of the weighted regression process for quantification in the real samples is given, including all the equations used. Results from the injection time study (electropherograms and peak aras) are shown. We then show the approach we used to convert results from the TDAPS and HEPBS concentration studies to electrophoretic mobilities, how the mobilities are fit to theory to obtain association constants, and complete results for the TDAPS association constant measurements. After that, some discussion on and a table of measured detection limits are given. Next, additional discussion and electropherograms are provided for the interference testing. The last section then shows representative separations for the real samples with both the MCE and IC methods.

Weighted Regression Analysis

For the weighted linear regression and uncertainty calculations shown here, the sum of the weights has to be equal to the number of samples analyzed. The weights (w) are typically done as either the x- or y-values (generically 'z') to some power (generically 'p'). For 'n' calibration measurements, the weights are then given by equation 1.

$$w_i = \frac{n z_i^p}{\sum_{i=1}^{n} z_i^p} \quad \text{(eq 1)}$$

In this work, weighting is given to concentration (x) to the −1 power, resulting in eq 2.

$$w_i = \frac{n x_i^{-1}}{\sum_{i=1}^{n} x_i^{-1}} \quad \text{(eq 2)}$$

The slope (m) and intercept (b) are given by eq 3 and eq 4, respectively.

$$m = \frac{S_{xy}}{S_{xx}} \quad \text{(eq 3)}$$

$$b = \bar{y} - m\bar{x} \quad \text{(eq 4)}$$

The weighted x- and y-centroids are given by eq 5 and eq 6.

$$\bar{x} = \frac{\sum_{i=1}^{n} w_i x_i}{\sum_{i=1}^{n} w_i} \quad \text{(eq 5)}$$

$$\bar{y} = \frac{\sum_{i=1}^{n} w_i y_i}{\sum_{i=1}^{n} w_i} \quad \text{(eq 6)}$$

Weighted S_{xx} and S_{xy} are given by eq 7 and eq 8.

$$S_{xx} = \sum_i w_i \left(x_i - \bar{x}\right)^2 \quad \text{(eq 7)}$$

$$S_{xy} = \sum_i w_i \left(x_i - \bar{x}\right)\left(y_i - \bar{y}\right) \quad \text{(eq 8)}$$

The calibration data were analyzed using the above equations to obtain best-fit slopes and intercepts. From these, predicted y values ($\hat{y}$) for the calibration data were computed and then used to calculate the sum of the squares of the residuals, SS_E, using eq 9.

$$SS_E = \sum_i w_i \left(y_i - \hat{y}_i\right)^2 \quad \text{(eq 9)}$$

The confidence interval (CI) and prediction interval (PI) of the calibration were then computed as the best fit ± the values given in eq 10 and eq 11. The intervals depend on the relative x-distance between the current position (x_o) and the weighted calibration x-centroid. The prediction interval also depends on the weighting at that calibration point, w_o, which can be computed using eq 12 (where the summation is only the calibration data).

$$CI = \pm t_{\alpha/2,DOF}\hat{s}\sqrt{\frac{1}{n}+\frac{\left(x_o-\bar{x}\right)^2}{S_{xx}}} \quad \text{(eq 10)}$$

$$PI = \pm t_{\alpha/2,DOF}\hat{s}\sqrt{\frac{1}{w_o}+\frac{1}{n}+\frac{\left(x_o-\bar{x}\right)^2}{S_{xx}}} \quad \text{(eq 11)}$$

$$w_o = \frac{nx_o^{-1}}{\sum_{i=1}^{n} x_i^{-1}} \quad \text{(eq 12)}$$

Here, $t_{\alpha/2,DOF}$ is the upper α/2 fraction of the *t* distribution. Degrees of freedom (DOF) equals n-2 for linear fits with non-fixed slopes and intercepts. ŝ is a function of SS_E, as given by eq 13.

$$\hat{s} = \sqrt{\frac{SS_E}{DOF}} \quad \text{(eq 13)}$$

For polynomial regression, calibration weighting was done using eq 2. The polynomial fit and CI were calculated with OriginPro 8.0 using direct weighting. The PI was then calculated from the CI produced from OriginPro using eq 14 where w_o is computed using eq 12.

$$PI = \pm t_{\alpha/2,DOF}\hat{s}\sqrt{\left(\frac{CI}{t_{\alpha/2,DOF}\hat{s}}\right)^2+\frac{1}{w_o}} \quad \text{(eq 14)}$$

The DOF is equal to n minus the number of adjustable parameter, so n-3 with the 2nd order polynomial fits. Eqs 6, 9, and 13 are used as-is for computing the necessary values in eq 14.

Injection Time Study

For highest-precision injections, injections need to be long enough that there is low sensitivity of the injected quantity to injection time (or matrix) variations. Therefore, an injection time study was performed using BGE 1 and 10-μM analytes (the ten species shown in the top trace of Figure 3). Tested injections ranged from 4 to 45 sec. Four replicates were performed and averaged for each injection time. Representative electropherograms are shown in Figure S-1. Peak areas for the study are shown in Figure S-2. All of the species except selenite showed little variation after ~20 s, and selenite only showed a weak dependence at longer times, so a time of 30 s was chosen.

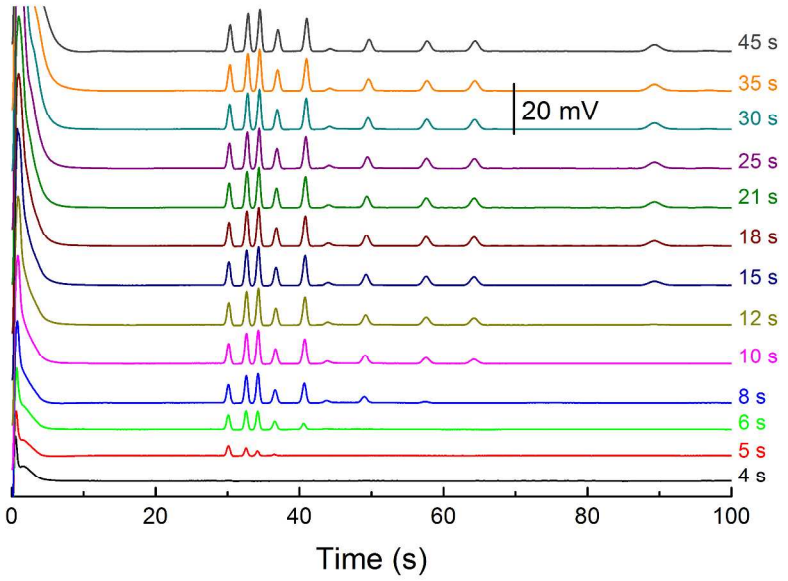

Figure S-1. Injection time study electropherograms. BGE 1 and 10-µM analytes used. Injection times are given on the right. Peak identities are the same as reported for the top trace in Figure 3.

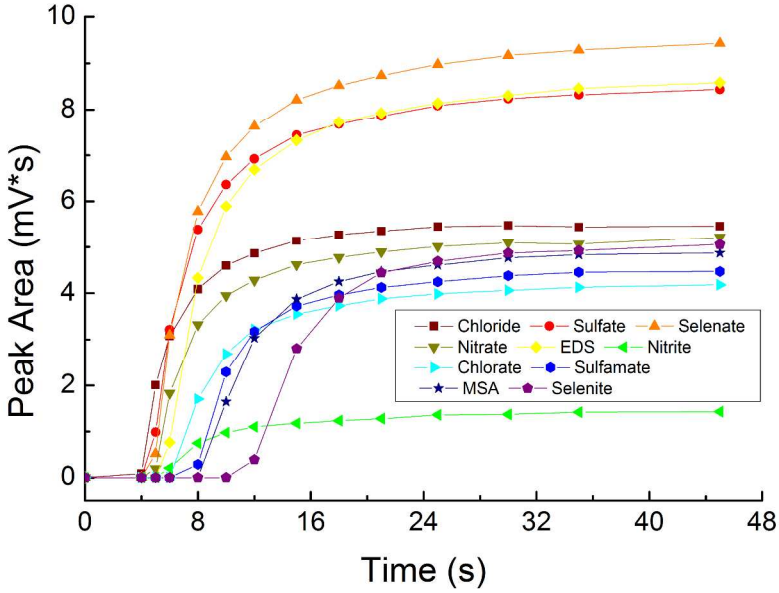

Figure S-2. Injection time study peak areas. Values are the average of four injections. BGE 1 and 10-µM analytes used.

TDAPS and HEBPS Binding Studies

The procedure used for measuring the mobilities of the analytes and fitting association constants (K) was modeled after the approach from reference 61. To compute the mobilities and display them in an intuitive way, the flow diagram in Scheme 1 was used. First, the separation was simulated using PeakMaster 5.2 software with the goal of obtaining the predicted mobility for sulfamate, the internal standard. Sulfamate was chosen because its interactions with HEPBS and

TDAPS are weak. Sulfamate's electrophoretic mobility (μ) was then adjusted for viscosity differences because PeakMaster 5.2 assumes a viscosity equal to water at 25 °C. Viscosity adjustments were a simple ratio (eq 15, where η is viscosity and the subscripts SIM and EXP are for the simulation and experimental viscosities, respectively) because mobility is inversely proportional to viscosity.

$$\mu = \frac{\mu_{SIM}\eta_{SIM}}{\eta_{EXP}} \qquad \text{(eq 15)}$$

Viscosity was measured using a U-tube viscometer. For the HEPBS study, this correction was only for temperature because the viscosity did not significantly change with HEPBS concentration. However, for the TDAPS study, the viscosity did change significantly with concentration. After compensating for viscosity, the electroosmotic mobility (μ_{EOF}) was calculated from sulfamate's migration time (t) using its viscosity-corrected predicted μ, the effective separation length (L_{eff}, 7 cm), the effective separation voltage (V_{eff}, −2763 V), and eq 16.

$$\mu_{EOF} = \frac{L_{eff}^2}{V_{eff}t} - \mu \qquad \text{(eq 16)}$$

This μ_{EOF} was used to calculate the electrophoretic mobilities of the other anions. Finally, these electrophoretic mobilities were adjusted for viscosity so that they were representative of what would be observed at a constant viscosity equal to that of water at 25 °C. This final viscosity correction was done both for visual appeal when plotting and for the calculation of K values because the value of interest is the hydrated radius, which is not directly affected by viscosity, rather than the actual mobility.

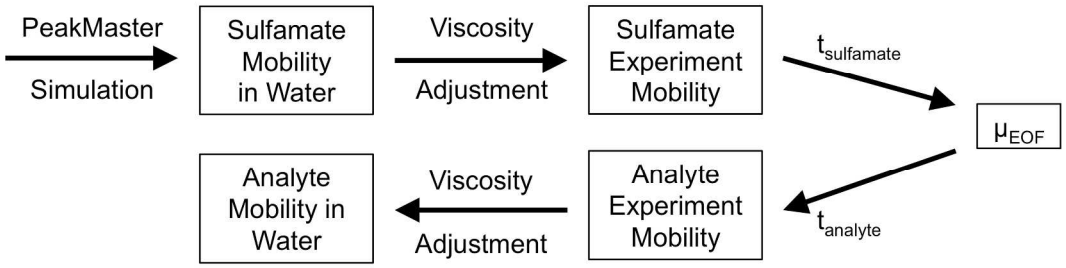

Scheme S-1. Approach for converting raw data to electrophoretic mobilities.

The approach used for calculating K values was similar to the method used in reference 61. The viscosity-corrected mobilities were fit to eq 17 with non-linear regression using OriginPro software. The ligand concentration, L, was the independent variable, μ was the dependent variable, and K, the unbound mobility (μ_0), and the bound mobility (μ_b) were the fitted parameters.

$$\mu = \mu_0 + (\mu_b - \mu_0)\frac{K[L]}{1 + K[L]} \qquad \text{(eq 17)}$$

For the TDAPS study, only nitrate, chlorate, and TFA were bound sufficiently for a reliable estimate of μ_b. For the remaining species, μ_b was fixed as the average bound mobility of nitrate, chlorate, and TFA multiplied by the analyte charge, and the resulting values were -3.4×10^{-5} and -6.8×10^{-5} cm^2 V^{-1} s^{-1} for mono- and dianions, respectively. For the HEPBS study, μ_b was estimated using equation 3 from reference 61, given here as eq 18, where *z* is the species' charge,

subscript L is the ligand (HEPBS), subscript S is the substrate (dianion), and subscript SL is the bound complex. Here, $z_{SL} = -1$, $z_L = +1$, $z_S = -2$, and $\mu_L = 2\times10^{-4}$ cm^2 V^{-1} s^{-1}. Values for μ_S were calculated from the data shown in Figure 2b.

$$\mu_b = \frac{2^{1/3} z_{SL} \mu_L \mu_S}{\sqrt[3]{2z_L^3 \mu_S^3 + z_S^3 \mu_L^3}} \quad \text{(eq 18)}$$

Full results from the TDAPS K measurements are shown in Table S-2. The confidence intervals shown are the non-linear regression uncertainties only and do not include other sources of uncertainty, specifically the uncertainties in V_{eff}, L_{eff}, viscosity measurements, temperature, or PeakMaster simulation of μ for sulfamate. The K value uncertainties might measurably increase if these uncertainties were added, but the mobility uncertainties would go up significantly and might be dominated by the non-fitting uncertainties. The fitting uncertainties for μ_0 were on the order of 10^{-7} cm^2 V^{-1} s^{-1} and therefore are not shown because non-fitting sources of uncertainty would entirely dominate. For instance, the contribution from only the PeakMaster simulation would be on the order of $\pm2\times10^{-6}$ cm^2 V^{-1} s^{-1}.

Table S-1. Measured Affinity Constants for TDAPS

Anion	K (M^{-1})	μ_b (10^{-5} cm^{2}V^{-1}s^{-1})	μ_o (10^{-4} cm^{2}V^{-1}s^{-1})	R^2
Chloride	0.34 (0.01)	−3.4*	−7.53	0.9889
Sulfate	~0	−6.8*	−7.29	--
Nitrate	5.25 (0.29)	−4.2 (3.1)	−7.02	0.99997
Selenate	~0	−6.8*	−6.94	--
Chlorate	12.84 (0.41)	−5.3 (1.3)	−6.28	0.99996
EDS	1.79 (0.01)	−6.8*	−6.19	0.99991
Nitrite	2.05 (0.02)	−3.4*	−5.99	0.9995
PDS	1.32 (0.01)	−6.8*	−5.63	0.9996
Methanesulfonate	0.24 (0.01)	−3.4*	−4.43	0.9849
TFA	14.38 (0.19)	−0.8 (0.4)	−4.04	>0.99999
Selenite	~0	−3.4*	−3.70	--

*Assumed as the average μ_b for nitrate, chlorate, and TFA multipled by the ion charge
Parenthetical values are half-widths of 95% confidence intervals

Complete Detection Limit Results

The main text only included detection limits for selenate and selenite. Table S-2 shows the measured detection limits for all of the species monitored by BGE 1. The high values for chloride and nitrite are due to very high blanks and wall adsorption, respectively. LOD measurements were made by measuring eight concentrations ranging from around 3× the LOD to slightly below the LOD (3 replicates), fitting a linear regression to the measured peak heights, and calculating where the regression line equaled the value of 2 digital-analog baseline steps (two steps = 0.101 mV). Sensitivity (slope of the regression line) is also provided in Table S-2 and can be used to estimate LOD for the ubiquitous species if blank measurements could be reduced to negligible values.

Table S-2. Measured Detection Limits

Anion	Sensitivity (mV/µM)	LOD (nM)
Chloride	0.84	1900*
Sulfate	1.60	200*
Selenate	1.95	53
Nitrate	0.74	140*
Nitrite	0.18	610
Chlorate	0.50	210
Sulfamate	0.47	240
Methanesulfonate	0.41	240*
Selenite	0.25	380

*Calculated as 3σ of the blank instead of from baseline noise

Weak Acid Interference Testing

Common weak acids, mostly organic, that were tested for interfering with BGE 1 were fluoride, formate, pyruvate, malonate, fumarate, tartrate, and oxalate. Oxalate was not observed in the electropherograms, likely due to wall adsorption. The other species were observed, though pyruvate and malonate presented distorted and/or tailing peaks. The results from the interference testing are shown in Figure S-3.

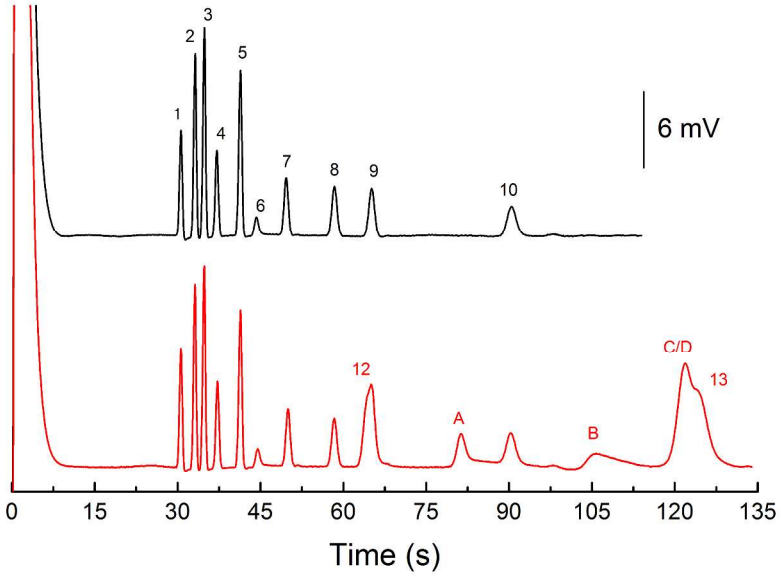

Figure S-3. Top: 10-µM analytes separated with BGE 1. Identities: 1, chloride; 2, sulfate; 3, selenate; 4, nitrate; 5, EDS (standard); 6, nitrite; 7, chlorate; 8, sulfamate; 9, methanesulfonate; 10, selenite. Bottom: 10-µM analytes from the top trace with 20-µM potentially interfering species. Identities: 12, fluoride; 13, formate; A, pyruvate; B, malonate; C, fumarate; D, tartrate.

Representative Real Sample Separations

The dilute BBL broth samples were analyzed by both MCE and IC and constitute a good test of the selectivity and resilience of the methods to complicated matrices. The quantitative results from the analysis were shown in the main text. Examination of the electropherograms and

chromatograms is also useful because it clarifies how selective the methods are to interfering species, how stable the baselines are, and how long the analyses take. Figure S-4 shows a BBL broth blank and spiked sample for MCE. Figure S-5 shows the IC equivalents for these two analyses.

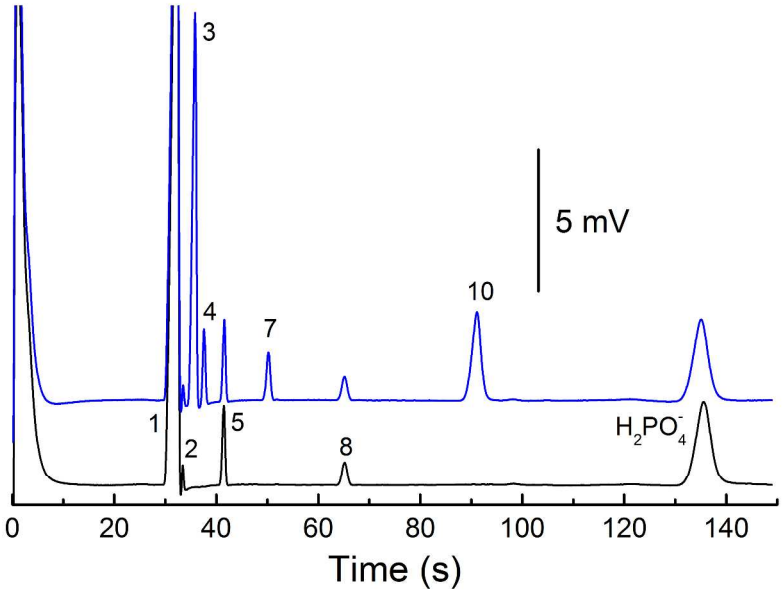

Figure S-4. MCE analysis of BBL broth samples using BGE 1. Top: electropherogram of 0.5% BBL broth blank (real sample 1). Bottom: electropherogram of real sample 4 (diluted ~10× in 0.5% broth). Peak identity numbers are the same as shown in Figure 3. Sample concentrations are given in Table 1. Internal standards were 10 μM.

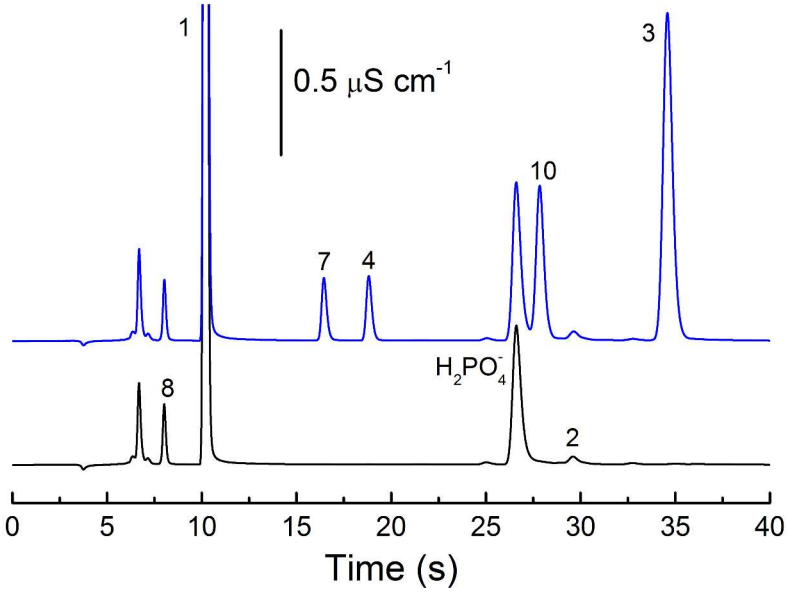

Figure S-5. IC analysis of BBL broth samples. Top: chromatogram of 0.5% BBL broth blank (real sample 1). Bottom: chromatogram of real sample 6 (diluted ~10× in 0.5% broth). Peak identity numbers are the same as in Figure 3. Methanesulfonate standard was 10 μM. The peak(s) at ~7 min are unknown(s).